

Quantum Field Theory on a Highly Symmetric Lattice

Marco Aliberti

Università degli Studi di Torino

23rd October, 2023

The Strong Interaction

Matter is made of Atoms

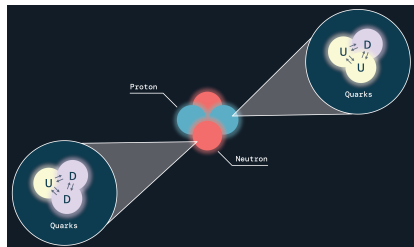


Image credits: NASA^[NASA, 2022]

The Strong Interaction

Matter is made of Atoms

Atoms are made of Nuclei and Electrons

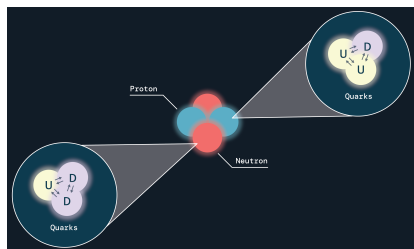


Image credits: NASA^[NASA, 2022]

The Strong Interaction

Matter is made of Atoms

Atoms are made of Nuclei and Electrons

Nuclei are made of Protons and Neutrons,
composed of Quarks and Gluons

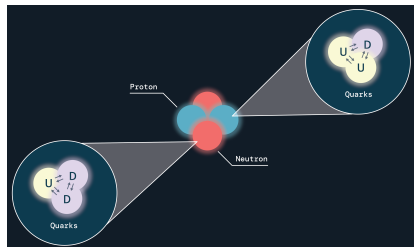


Image credits: NASA^[NASA, 2022]

The Strong Interaction

Matter is made of Atoms

Atoms are made of Nuclei and Electrons

Nuclei are made of Protons and Neutrons,
composed of Quarks and Gluons

Quarks and Gluons

Described by Quantum
Chromodynamics (QCD)

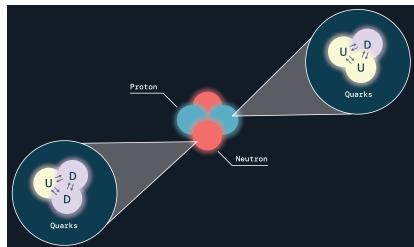


Image credits: NASA^[NASA, 2022]

Quantum Chromodynamics (QCD)

Described by an $SU(3)$ Yang-Mills theory

$$S = \frac{1}{4} \int d^4x F_{\mu\nu}^a(x) F^{a\mu\nu}(x)$$

$$F_{\mu\nu}^a = \partial_\mu A_\nu^a - \partial_\nu A_\mu^a - gf_{bc}^a A_\mu^b A_\nu^c$$

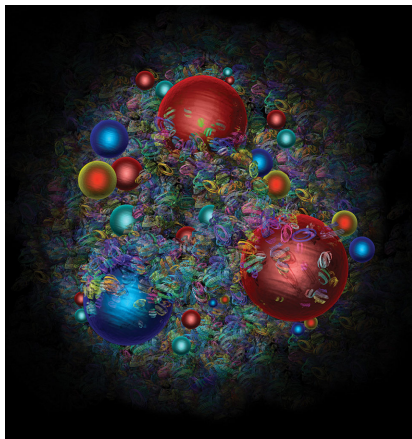


Figure: An artist's representation of a proton^[CERN, 2019].

Quantum Chromodynamics (QCD)

Described by an $SU(3)$ Yang-Mills theory

$$S = \frac{1}{4} \int d^4x F_{\mu\nu}^a(x) F^{a\mu\nu}(x)$$

$$F_{\mu\nu}^a = \partial_\mu A_\nu^a - \partial_\nu A_\mu^a - gf_{bc}^a A_\mu^b A_\nu^c$$

- 3 color charges

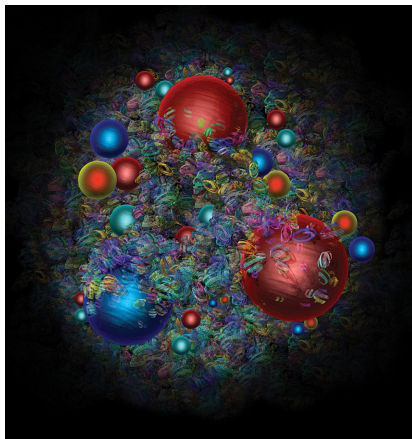


Figure: An artist's representation of a proton^[CERN, 2019].

Quantum Chromodynamics (QCD)

Described by an $SU(3)$ Yang-Mills theory

$$S = \frac{1}{4} \int d^4x F_{\mu\nu}^a(x) F^{a\mu\nu}(x)$$

$$F_{\mu\nu}^a = \partial_\mu A_\nu^a - \partial_\nu A_\mu^a - gf_{bc}^a A_\mu^b A_\nu^c$$

- 3 color charges
- Interesting purely-gluonic physics

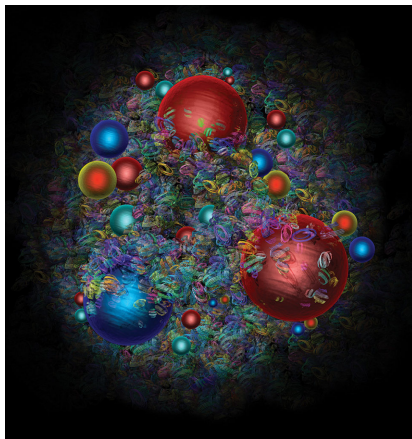


Figure: An artist's representation of a proton [CERN, 2019].

Quantum Chromodynamics (QCD)

Described by an $SU(3)$ Yang-Mills theory

$$S = \frac{1}{4} \int d^4x F_{\mu\nu}^a(x) F^{a\mu\nu}(x)$$

$$F_{\mu\nu}^a = \partial_\mu A_\nu^a - \partial_\nu A_\mu^a - gf_{bc}^a A_\mu^b A_\nu^c$$

- 3 color charges
- Interesting purely-gluonic physics
- Heavily non-perturbative nature (except for specific regimes)

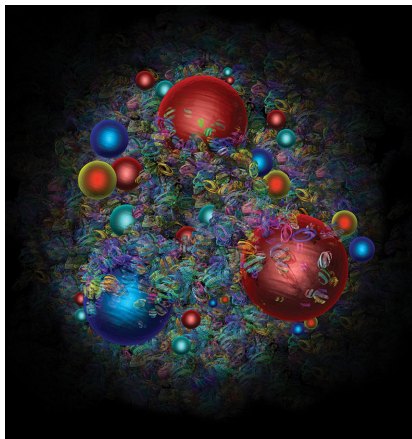


Figure: An artist's representation of a proton [CERN, 2019].

Quantum Chromodynamics (QCD)

Described by an $SU(3)$ Yang-Mills theory

$$S = \frac{1}{4} \int d^4x F_{\mu\nu}^a(x) F^{a\mu\nu}(x)$$

$$F_{\mu\nu}^a = \partial_\mu A_\nu^a - \partial_\nu A_\mu^a - gf_{bc}^a A_\mu^b A_\nu^c$$

- 3 color charges
- Interesting purely-gluonic physics
- Heavily non-perturbative nature (except for specific regimes)



Lattice Field Theory

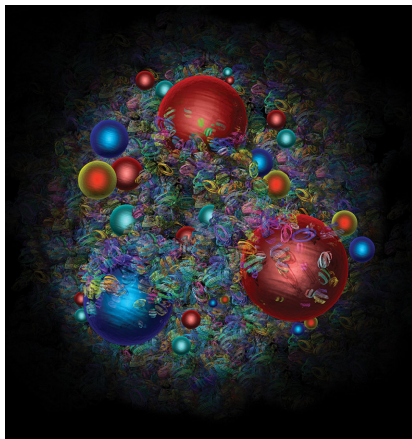


Figure: An artist's representation of a proton^[CERN, 2019].

What is a Lattice?

Definition: Lattice Λ

$\Lambda = \{ \sum_{i=1}^n a_i e_i \mid a_i \in \mathbb{Z} \}$, with $\{e_i\}$ any basis of \mathbb{R}^n

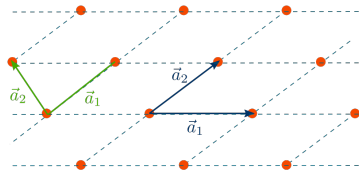


Figure: A bidimensional lattice.

What is a Lattice?

Definition: Lattice Λ

$\Lambda = \{ \sum_{i=1}^n a_i e_i \mid a_i \in \mathbb{Z} \}$, with $\{e_i\}$ any basis of \mathbb{R}^n

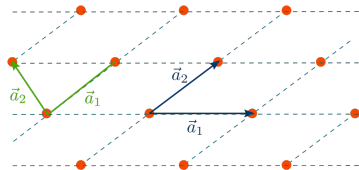


Figure: A bidimensional lattice.

Hypercubic lattice

$\{e_i\}$ is the canonical basis of \mathbb{R}^n
 a is called *lattice spacing*.

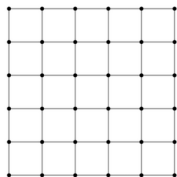


Figure: A square lattice.

Basic idea

Fields can take values only in given parts of the lattice, $x \rightarrow n \in \Lambda$.

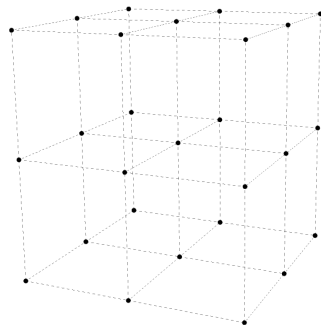


Figure: A (hyper)cubic lattice in \mathbb{R}^3 .

Basic idea

Fields can take values only in given parts of the lattice, $x \rightarrow n \in \Lambda$.

Examples:

- **Scalar fields** $\Phi(x) \rightarrow \Phi(n)$ on sites

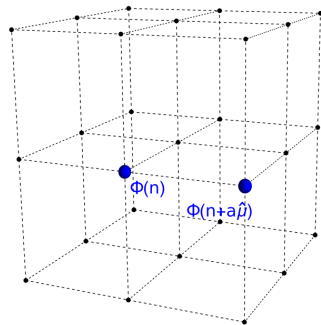


Figure: A (hyper)cubic lattice in \mathbb{R}^3 .

Basic idea

Fields can take values only in given parts of the lattice, $x \rightarrow n \in \Lambda$.

Examples:

- **Scalar fields** $\Phi(x) \rightarrow \Phi(n)$ on sites
- **Vector fields** $U_\mu(x) \rightarrow U_\mu(n)$ on links

Parallel Transporter

$$U_\mu(x) = \exp(igaA_\mu(x))$$

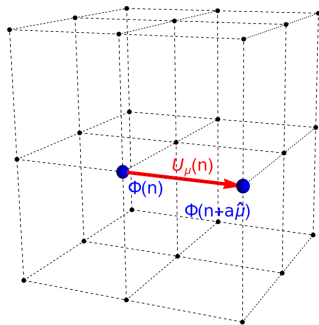


Figure: A (hyper)cubic lattice in \mathbb{R}^3 .

Basic idea

Fields can take values only in given parts of the lattice, $x \rightarrow n \in \Lambda$.

Examples:

- **Scalar fields** $\Phi(x) \rightarrow \Phi(n)$ on sites
- **Vector fields** $U_\mu(x) \rightarrow U_\mu(n)$ on links
- Object with k indices on k -simplexes

Parallel Transporter

$$U_\mu(x) = \exp(igaA_\mu(x))$$

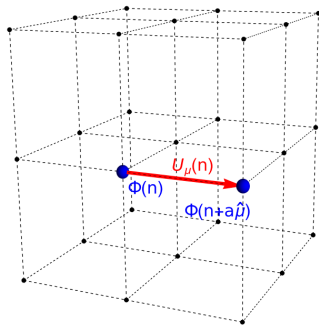


Figure: A (hyper)cubic lattice in \mathbb{R}^3 .

Basic idea

Fields can take values only in given parts of the lattice, $x \rightarrow n \in \Lambda$.

Examples:

- **Scalar fields** $\Phi(x) \rightarrow \Phi(n)$ on sites
- **Vector fields** $U_\mu(x) \rightarrow U_\mu(n)$ on links
- Object with k indices on k -simplexes

Beware!

Spinorial fields are trickier to be discretized.

Parallel Transporter

$$U_\mu(x) = \exp(igaA_\mu(x))$$

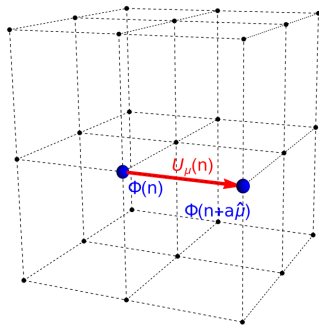


Figure: A (hyper)cubic lattice in \mathbb{R}^3 .

Gauge-Invariant Observables and Wilson Action

The Yang-Mills continuum action is
$$S_E = \frac{1}{4} \int d^4x F^{a\mu\nu}(x) F_{\mu\nu}^a(x).$$

On the lattice, every closed path is gauge-invariant.

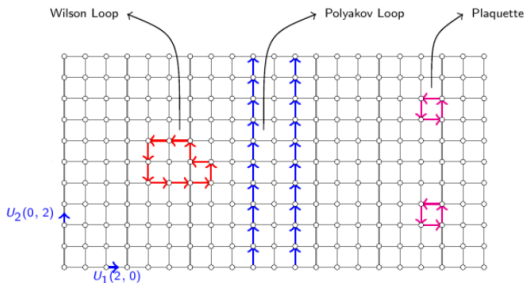


Figure: Gauge-invariant paths on a bidimensional lattice [Sigdel, 2016].

Gauge-Invariant Observables and Wilson Action

The Yang-Mills continuum action is
$$S_E = \frac{1}{4} \int d^4x F^{a\mu\nu}(x) F_{\mu\nu}^a(x).$$

On the lattice, every closed path is gauge-invariant.

Definition: Plaquette $U_{\mu\nu}(n)$

$$U_\mu(n) U_\nu(n + \mu) U_\mu^\dagger(n + \nu) U_\nu^\dagger(n)$$

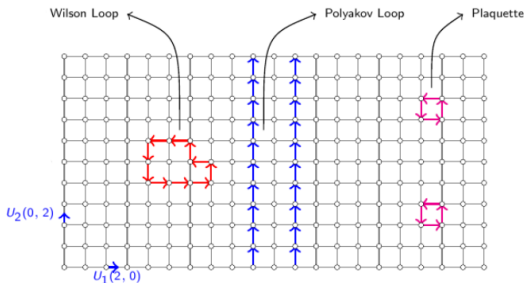


Figure: Gauge-invariant paths on a bidimensional lattice [Sigdel, 2016].

Gauge-Invariant Observables and Wilson Action

The Yang-Mills continuum action is
$$S_E = \frac{1}{4} \int d^4x F^{a\mu\nu}(x) F_{\mu\nu}^a(x).$$

On the lattice, every closed path is gauge-invariant.

Definition: Plaquette $U_{\mu\nu}(n)$

$$U_\mu(n) U_\nu(n + \mu) U_\mu^\dagger(n + \nu) U_\nu^\dagger(n)$$

Wilson's Idea

$$S = \frac{\beta}{2N} \sum_{n,\mu,\nu} \Re \text{Tr} (1 - U_{\mu\nu}(n))$$

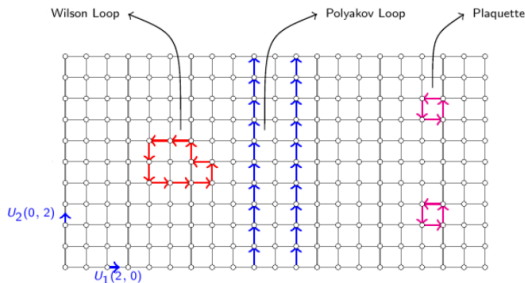


Figure: Gauge-invariant paths on a bidimensional lattice^[Sigdel, 2016].

Polyakov Loops and Potential

If the time coordinate is taken to be periodic, more closed paths arise.

Polyakov Loop

$$P(n) = \text{Tr} \prod_{t=0}^{T-1} U_t(n)$$

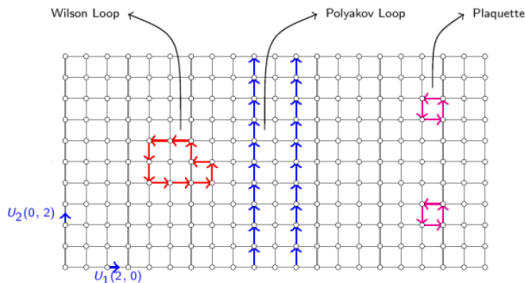


Figure: Gauge-invariant paths on a bidimensional lattice [Sigdel, 2016].

Polyakov Loops and Potential

If the time coordinate is taken to be periodic, more closed paths arise.

The expectation value of two Polyakov loops is the potential.

Polyakov Loop

$$P(n) = \text{Tr} \prod_{t=0}^{T-1} U_t(n)$$

Potential

$$V(R) = -\frac{1}{T} \log \langle P(0) P^\dagger(R) \rangle$$

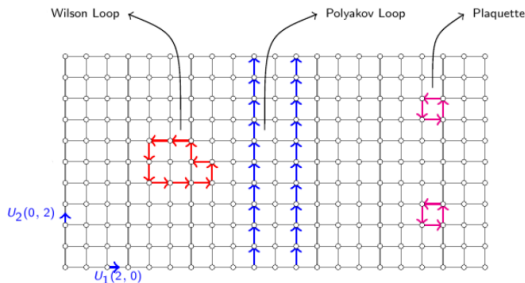


Figure: Gauge-invariant paths on a bidimensional lattice [Sigdel, 2016].

Monte Carlo Simulations

Computers are used to simulate Lattice Field Theories



Figure: A rendering of the CINECA Leonardo supercomputer^[Wikipedia, 2022].

Monte Carlo Simulations

Computers are used to simulate Lattice Field Theories

- Random configurations of link variables are generated.



Figure: A rendering of the CINECA Leonardo supercomputer^[Wikipedia, 2022].

Monte Carlo Simulations

Computers are used to simulate Lattice Field Theories

- Random configurations of link variables are generated.
- Proper Monte Carlo algorithms evolve the configurations towards minimums of the action.



Figure: A rendering of the CINECA Leonardo supercomputer^[Wikipedia, 2022].

Monte Carlo Simulations

Computers are used to simulate Lattice Field Theories

- Random configurations of link variables are generated.
- Proper Monte Carlo algorithms evolve the configurations towards minimums of the action.
- A great number of observables is evaluated and then their mean value is computed.



Figure: A rendering of the CINECA Leonardo supercomputer^[Wikipedia, 2022].

Poincaré Group can be divided in:

Translations

Rotations

Poincaré Group can be divided in:

Translations

$$x^\mu \rightarrow x^\mu + \varepsilon^\mu$$

\Downarrow

$$n \rightarrow n + a\hat{\mu}$$

Rotations

Poincaré Group can be divided in:

Translations

$$x^\mu \rightarrow x^\mu + \varepsilon^\mu$$

\Downarrow

$$n \rightarrow n + a\hat{\mu}$$

Rotations

$$x^\mu \rightarrow R^\mu_\nu x^\nu \quad R \in SO(4)$$

\Downarrow

$$n \rightarrow \Gamma n \quad \Gamma \in G_{\Lambda_{SH}}$$

$G_{\Lambda_{SH}}$: group of rotations of multiples of 90° around any axis.

Poincaré Group can be divided in:

Translations

$$x^\mu \rightarrow x^\mu + \varepsilon^\mu$$

\Downarrow

$$n \rightarrow n + a\hat{\mu}$$

$$a\hat{\mu} \rightarrow \varepsilon^\mu \text{ for } a \rightarrow 0$$

Rotations

$$x^\mu \rightarrow R^\mu_\nu x^\nu \quad R \in SO(4)$$

\Downarrow

$$n \rightarrow \Gamma n \quad \Gamma \in G_{\Lambda_{SH}}$$

$G_{\Lambda_{SH}}$: group of rotations of multiples of 90° around any axis.

Lattice Symmetries

Poincaré Group can be divided in:

Translations

$$x^\mu \rightarrow x^\mu + \varepsilon^\mu$$

\Downarrow

$$n \rightarrow n + a\hat{\mu}$$

$$a\hat{\mu} \rightarrow \varepsilon^\mu \text{ for } a \rightarrow 0$$

Rotations

$$x^\mu \rightarrow R^\mu_\nu x^\nu \quad R \in SO(4)$$

\Downarrow

$$n \rightarrow \Gamma n \quad \Gamma \in G_{\Lambda_{SH}}$$

$G_{\Lambda_{SH}}$: group of rotations of multiples of 90° around any axis.

$$\Gamma \rightarrow R \text{ for } a \rightarrow 0$$

Lattice Symmetries

Poincaré Group can be divided in:

Translations

$$x^\mu \rightarrow x^\mu + \varepsilon^\mu$$



$$n \rightarrow n + a\hat{\mu}$$

$$a\hat{\mu} \rightarrow \varepsilon^\mu \text{ for } a \rightarrow 0$$

Rotations

$$x^\mu \rightarrow R^\mu_\nu x^\nu \quad R \in SO(4)$$



$$n \rightarrow \Gamma n \quad \Gamma \in G_{\Lambda_{SH}}$$

$G_{\Lambda_{SH}}$: group of rotations of multiples of 90° around any axis.

$$\Gamma \not\rightarrow R \text{ for } a \rightarrow 0$$

Important:

Rotational invariance seems to be broken.

Rotational Invariance Restoration - Lang and Rebbi

Equipotential surfaces become spheres as the continuum limit is approached^[Lang and Rebbi, 1982].

The gauge group used was the discrete icosahedral subgroup $\tilde{Y} \subset SU(2)$.

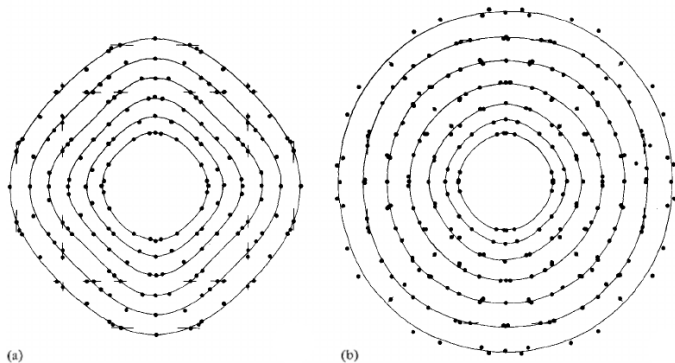


Figure: Restoration of rotational invariance from (a) $\beta = 2$, $n_s = 8$, $n_t = 4$ to (b) $\beta = 2.25$, $n_s = 16$, $n_t = 6$; the curves represent equipotential curves.

Rotational Invariance Restoration

Results of simulations for gauge group $SU(2)$ with 20000 measurements each¹. Approach slightly different than Lang and Rebbi's.

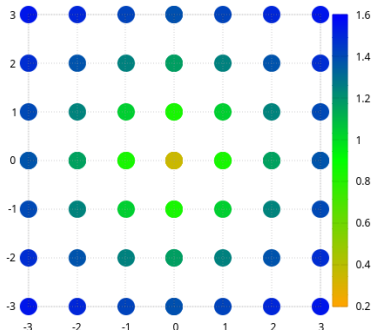


Figure: Potential from $\beta = 2.20$,
 $n_s = 8$, $n_t = 4$.

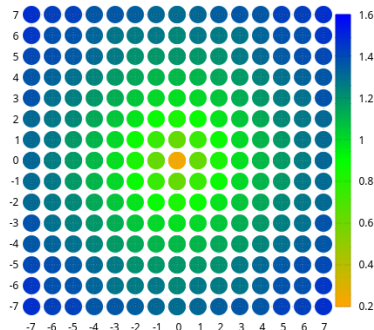


Figure: Potential from $\beta = 2.35$,
 $n_s = 16$, $n_t = 6$.

¹The simulation code is based on the code presented in refs. [Panero, 2009; Mykkänen, Panero, and Rummukainen, 2012].

Higher Symmetry Lattices

Other, more rotational-symmetric, lattices have been used:

Body Centered Tesseract

- 24 nearest neighbours
- 1152-element symmetry group

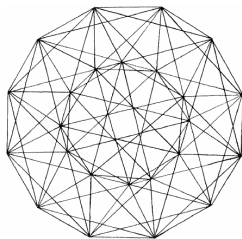


Figure: Two-dimensional projection of a BCT^[Celmaster, 1982].

The SH lattice has 8 nearest neighbours and a 384-element symmetry group.

Higher Symmetry Lattices

Other, more rotational-symmetric, lattices have been used:

Body Centered Tesseract

- 24 nearest neighbours
- 1152-element symmetry group

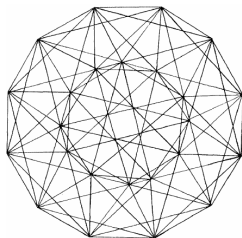


Figure: Two-dimensional projection of a BCT^[Celmaster, 1982].

F_4 coroots lattice^[Neuberger, 1987]

- 48 nearest neighbours
- 2304-element symmetry group

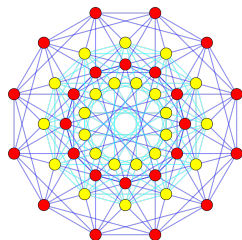


Figure: Two-dimensional projection of a F_4 coroots lattice^[Wikipedia, 2010].

The SH lattice has 8 nearest neighbours and a 384-element symmetry group.

Body Centered Tesseract (BCT)

- Obtained from Simple Hypercubic lattice considering also the centers;

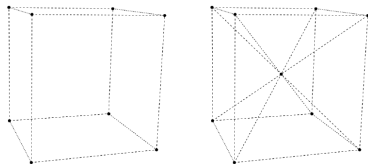


Figure: Cubic Cell (left) and BC Cubic Cell (right).

Body Centered Tesseract (BCT)

- Obtained from Simple Hypercubic lattice considering also the centers;
- Elementary cell is the 24-cell;

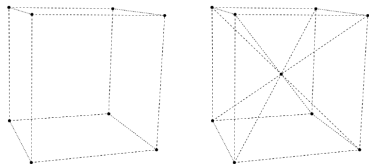


Figure: Cubic Cell (left) and BC Cubic Cell (right).

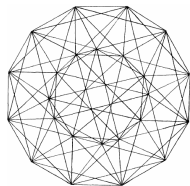


Figure: Bidimensional projection of the 24-cell.

Body Centered Tesseract (BCT)

- Obtained from Simple Hypercubic lattice considering also the centers;
- Elementary cell is the 24-cell;
- Has 24 nearest neighbours:
 - The 8 possible permutations of $(\pm 1, 0, 0, 0)$
 - The 16 vectors of the form $(\pm \frac{1}{2}, \pm \frac{1}{2}, \pm \frac{1}{2}, \pm \frac{1}{2})$

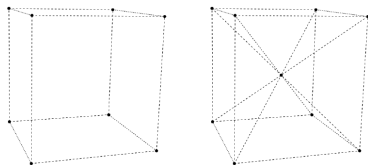


Figure: Cubic Cell (left) and BC Cubic Cell (right).

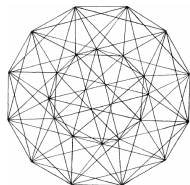


Figure: Bidimensional projection of the 24-cell.

Body Centered Tesseract (BCT)

- Obtained from Simple Hypercubic lattice considering also the centers;
- Elementary cell is the 24-cell;
- Has 24 nearest neighbours:
 - The 8 possible permutations of $(\pm 1, 0, 0, 0)$
 - The 16 vectors of the form $(\pm \frac{1}{2}, \pm \frac{1}{2}, \pm \frac{1}{2}, \pm \frac{1}{2})$
- Plaquettes are triangular;

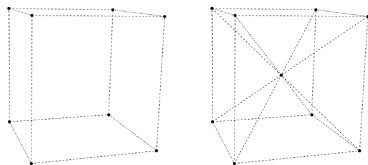


Figure: Cubic Cell (left) and BC Cubic Cell (right).

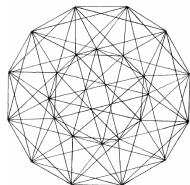


Figure: Bidimensional projection of the 24-cell.

Body Centered Tesseract (BCT)

- Obtained from Simple Hypercubic lattice considering also the centers;
- Elementary cell is the 24-cell;
- Has 24 nearest neighbours:
 - The 8 possible permutations of $(\pm 1, 0, 0, 0)$
 - The 16 vectors of the form $(\pm \frac{1}{2}, \pm \frac{1}{2}, \pm \frac{1}{2}, \pm \frac{1}{2})$
- Plaquettes are triangular;
- Contains the Simple Hypercubic lattice;

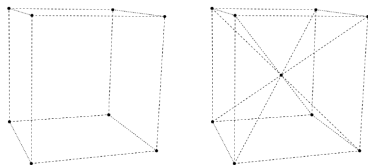


Figure: Cubic Cell (left) and BC Cubic Cell (right).

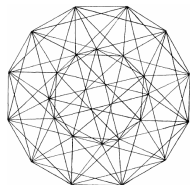


Figure: Bidimensional projection of the 24-cell.

Body Centered Tesseract (BCT)

- Obtained from Simple Hypercubic lattice considering also the centers;
- Elementary cell is the 24-cell;
- Has 24 nearest neighbours:
 - The 8 possible permutations of $(\pm 1, 0, 0, 0)$
 - The 16 vectors of the form $(\pm \frac{1}{2}, \pm \frac{1}{2}, \pm \frac{1}{2}, \pm \frac{1}{2})$
- Plaquettes are triangular;
- Contains the Simple Hypercubic lattice;
- Has been used to simulate $SU(2)$ Yang-Mills theories, in [Celmaster, 1982].

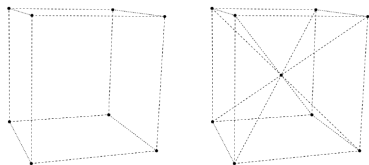


Figure: Cubic Cell (left) and BC Cubic Cell (right).

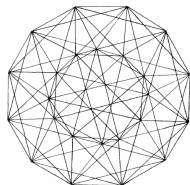


Figure: Bidimensional projection of the 24-cell.

F_4 Coroots Lattice

- Obtained from the roots lattice of the exceptional Lie algebra F_4 and its dual;

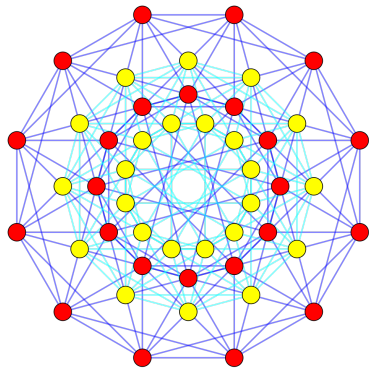


Figure: Bidimensional projection of the F_4 lattice.

F_4 Coroots Lattice

- Obtained from the roots lattice of the exceptional Lie algebra F_4 and its dual;
- Has 48 nearest neighbours:
 - The 24 roots are all possible permutations of coordinate positions of $(\pm 1, \pm 1, 0, 0)$

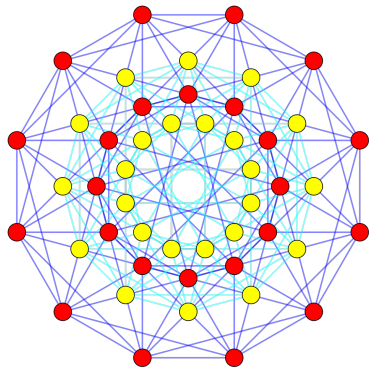


Figure: The 24 roots (red) of the F_4 lattice, projected on a bidimensional plane.

F_4 Coroots Lattice

- Obtained from the roots lattice of the exceptional Lie algebra F_4 and its dual;
- Has 48 nearest neighbours:
 - The 24 roots are all possible permutations of coordinate positions of $(\pm 1, \pm 1, 0, 0)$
 - The 24 dual roots (coroots) are:
 - The 8 possible permutations of $(\pm 1, 0, 0, 0)$
 - The 16 vectors of the form $(\pm \frac{1}{2}, \pm \frac{1}{2}, \pm \frac{1}{2}, \pm \frac{1}{2})$

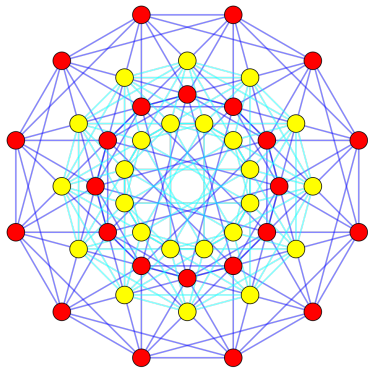


Figure: The 24 roots (red) and the 24 coroots (yellow) of the F_4 lattice, projected on a bidimensional plane.

F_4 Coroots Lattice

- Obtained from the roots lattice of the exceptional Lie algebra F_4 and its dual;
- Has 48 nearest neighbours:
 - The 24 roots are all possible permutations of coordinate positions of $(\pm 1, \pm 1, 0, 0)$
 - The 24 dual roots (coroots) are:
 - The 8 possible permutations of $(\pm 1, 0, 0, 0)$
 - The 16 vectors of the form $(\pm \frac{1}{2}, \pm \frac{1}{2}, \pm \frac{1}{2}, \pm \frac{1}{2})$
- Exists only in 4 dimensions;

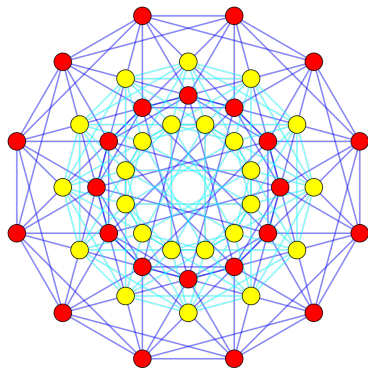


Figure: The 24 roots (red) and the 24 coroots (yellow) of the F_4 lattice, projected on a bidimensional plane.

F_4 Coroots Lattice

- Obtained from the roots lattice of the exceptional Lie algebra F_4 and its dual;
- Has 48 nearest neighbours:
 - The 24 roots are all possible permutations of coordinate positions of $(\pm 1, \pm 1, 0, 0)$
 - The 24 dual roots (coroots) are:
 - The 8 possible permutations of $(\pm 1, 0, 0, 0)$
 - The 16 vectors of the form $(\pm \frac{1}{2}, \pm \frac{1}{2}, \pm \frac{1}{2}, \pm \frac{1}{2})$
- Exists only in 4 dimensions;
- Is a more symmetric version of the BCT;

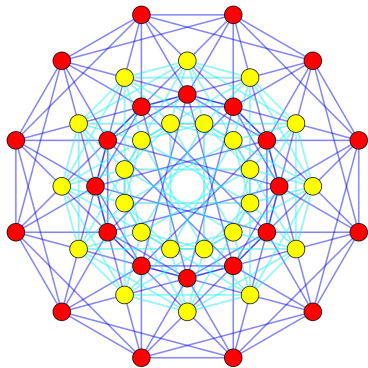


Figure: The 24 roots (red) and the 24 coroots (yellow) of the F_4 lattice, projected on a bidimensional plane.

F_4 Coroots Lattice

- Obtained from the roots lattice of the exceptional Lie algebra F_4 and its dual;
- Has 48 nearest neighbours:
 - The 24 roots are all possible permutations of coordinate positions of $(\pm 1, \pm 1, 0, 0)$
 - The 24 dual roots (coroots) are:
 - The 8 possible permutations of $(\pm 1, 0, 0, 0)$
 - The 16 vectors of the form $(\pm \frac{1}{2}, \pm \frac{1}{2}, \pm \frac{1}{2}, \pm \frac{1}{2})$
- Exists only in 4 dimensions;
- Is a more symmetric version of the BCT;
- Has been used only to simulate scalar fields, in [Neuberger, 1987].

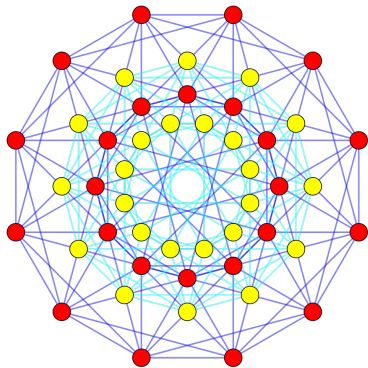


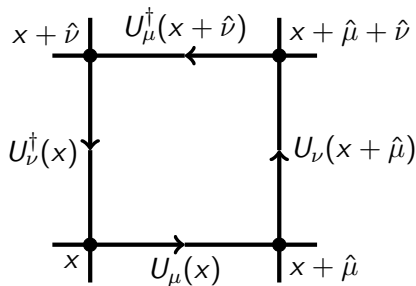
Figure: The 24 roots (red) and the 24 coroots (yellow) of the F_4 lattice, projected on a bidimensional plane.

Wilson Action:

$$S_W = \frac{\beta}{2N} \sum_{x \in \Lambda} \sum_{\mu < \nu} \Re \text{Tr}[\mathbb{1} - U_{\mu\nu}(x)]$$

Plaquette:

$$U_{\mu\nu} = U_\mu(x) U_\nu(x + \hat{\mu}) U_\mu^\dagger(x + \hat{\nu}) U_\nu^\dagger(x)$$



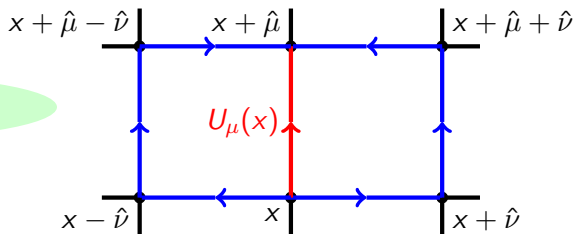
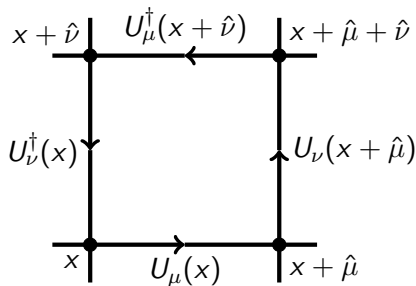
Simulations on SH Lattice

Wilson Action:

$$S_W = \frac{\beta}{2N} \sum_{x \in \Lambda} \sum_{\mu < \nu} \Re \text{Tr}[\mathbb{1} - U_{\mu\nu}(x)]$$

Plaquette:

$$U_{\mu\nu} = U_\mu(x) U_\nu(x + \hat{\mu}) U_\mu^\dagger(x + \hat{\nu}) U_\nu^\dagger(x)$$



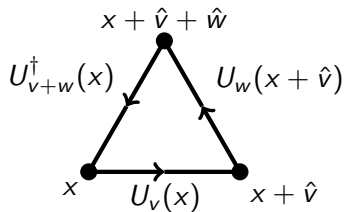
6 staples for each link

BCT Action:

$$S_{BCT} = \frac{\beta}{8} \sum_{\Delta} \Re \text{Tr } U_{\Delta}$$

Plaquette:

$$U_{\Delta} = U_v(x) U_w(x + \hat{v}) U_{v+w}^{\dagger}(x)$$



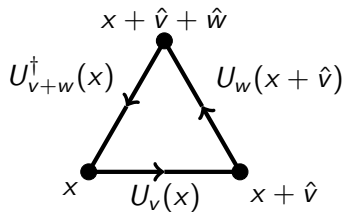
Simulations on BCT Lattice

BCT Action:

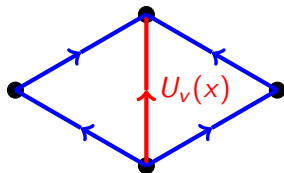
$$S_{BCT} = \frac{\beta}{8} \sum_{\Delta} \Re \text{Tr } U_{\Delta}$$

Plaquette:

$$U_{\Delta} = U_v(x) U_w(x + \hat{v}) U_{v+w}^{\dagger}(x)$$



8 staples for each link



Average Plaquette as a function of Computer Time

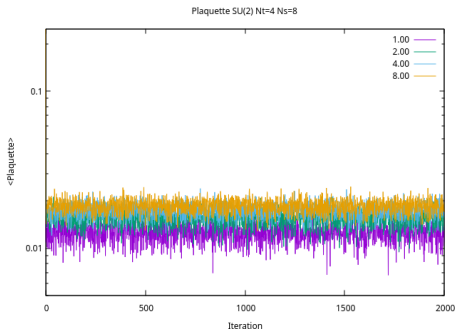


Figure: Lattice with $n_t = 4$, $n_s = 8$.

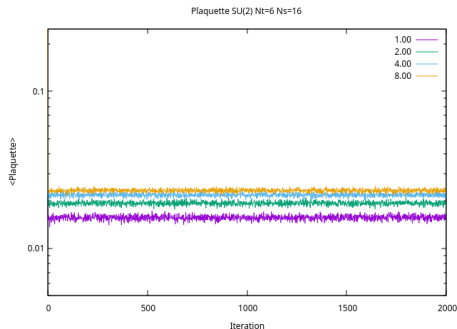
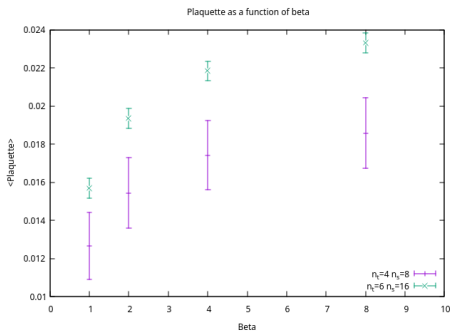


Figure: Lattice with $n_t = 6$, $n_s = 16$.

Average Plaquette as a function of β



Purple data is from a lattice with $n_t = 4$, $n_s = 8$.
Green data is from a lattice with $n_t = 6$, $n_s = 16$.

- Several tests of consistency (gauge invariance, plaquette correctness, etc.) have been successfully made;

Conclusions

- Several tests of consistency (gauge invariance, plaquette correctness, etc.) have been successfully made;
- Rapid convergence of the plaquette value has been observed;

Conclusions

- Several tests of consistency (gauge invariance, plaquette correctness, etc.) have been successfully made;
- Rapid convergence of the plaquette value has been observed;
- Plaquette value as a function of β do not show expected results:
 - Bigger error bars (w.r.t. SH lattice);

- Several tests of consistency (gauge invariance, plaquette correctness, etc.) have been successfully made;
- Rapid convergence of the plaquette value has been observed;
- Plaquette value as a function of β do not show expected results:
 - Bigger error bars (w.r.t. SH lattice);
 - Different trend than results obtained with different simulations in literature^[Celmaster, 1983];

- Several tests of consistency (gauge invariance, plaquette correctness, etc.) have been successfully made;
- Rapid convergence of the plaquette value has been observed;
- Plaquette value as a function of β do not show expected results:
 - Bigger error bars (w.r.t. SH lattice);
 - Different trend than results obtained with different simulations in literature^[Celmaster, 1983];
- Possible explanation: values of β used are far from the continuum limit (assuming there are no bugs in the code);

- Several tests of consistency (gauge invariance, plaquette correctness, etc.) have been successfully made;
- Rapid convergence of the plaquette value has been observed;
- Plaquette value as a function of β do not show expected results:
 - Bigger error bars (w.r.t. SH lattice);
 - Different trend than results obtained with different simulations in literature^[Celmaster, 1983];
- Possible explanation: values of β used are far from the continuum limit (assuming there are no bugs in the code);
- Extension to F_4 lattice would add "improvement terms" and more symmetries;

- Several tests of consistency (gauge invariance, plaquette correctness, etc.) have been successfully made;
- Rapid convergence of the plaquette value has been observed;
- Plaquette value as a function of β do not show expected results:
 - Bigger error bars (w.r.t. SH lattice);
 - Different trend than results obtained with different simulations in literature^[Celmaster, 1983];
- Possible explanation: values of β used are far from the continuum limit (assuming there are no bugs in the code);
- Extension to F_4 lattice would add "improvement terms" and more symmetries;
- Rotational invariance studies could be made.

Thank you for your attention

Bibliography I



NASA (2022). URL:

<https://universe.nasa.gov/resources/254/strong-force/>
(visited on 12/20/2022).



CERN (2019). URL:





<https://home.cern/news/news/physics/proton-century> (visited
on 06/12/2019).



Sigdel, Dibakar (2016). “Two Dimensional Lattice Gauge Theory with
and without Fermion Content”. In: *FIU Electronic Theses and
Dissertations* 3224. DOI: 10.25148/etd.FIDC001748. URL:
[https://digitalcommons.fiu.edu/etd/3224?utm_source=
digitalcommons.fiu.edu%2Fetd%2F3224&utm_medium=PDF&utm_
campaign=PDFCoverPages](https://digitalcommons.fiu.edu/etd/3224?utm_source=digitalcommons.fiu.edu%2Fetd%2F3224&utm_medium=PDF&utm_campaign=PDFCoverPages).



Wikipedia (2022). URL: [https://en.wikipedia.org/wiki/
Leonardo_\(supercomputer\)#/media/File:Modello_Leonardo.jpg](https://en.wikipedia.org/wiki/Leonardo_(supercomputer)#/media/File:Modello_Leonardo.jpg)
(visited on 09/25/2022).

-  Lang, C. B. and C. Rebbi (1982). “Potential and Restoration of Rotational Symmetry in SU(2) Lattice Gauge Theory”. In: *Phys. Lett.* B115. [, 322 (1982)], p. 137. DOI: [10.1016/0370-2693\(82\)90813-9](https://doi.org/10.1016/0370-2693(82)90813-9).
-  Panero, Marco (2009). “Thermodynamics of the QCD plasma and the large-N limit”. In: *Phys. Rev. Lett.* 103, p. 232001. DOI: [10.1103/PhysRevLett.103.232001](https://doi.org/10.1103/PhysRevLett.103.232001). arXiv: [0907.3719 \[hep-lat\]](https://arxiv.org/abs/0907.3719).
-  Mykkänen, Anne, Marco Panero, and Kari Rummukainen (2012). “Casimir scaling and renormalization of Polyakov loops in large-N gauge theories”. In: *JHEP* 1205, p. 069. DOI: [10.1007/JHEP05\(2012\)069](https://doi.org/10.1007/JHEP05(2012)069). arXiv: [1202.2762 \[hep-lat\]](https://arxiv.org/abs/1202.2762).
-  Celmaster, William (1982). “Gauge Theories on the Body - Centered Hypercubic Lattice”. In: *Phys. Rev.* D26, p. 2955. DOI: [10.1103/PhysRevD.26.2955](https://doi.org/10.1103/PhysRevD.26.2955).



Neuberger, Herbert (1987). “SPINLESS FIELDS ON $F(4)$ LATTICES”. In: *Phys. Lett. B* 199, pp. 536–540. DOI: 10.1016/0370-2693(87)91623-6.



Wikipedia (2010). URL: https://en.wikipedia.org/wiki/F4_%28mathematics%29#/media/File:F4_roots_by_24-cell_duals.svg (visited on 12/13/2010).



Celmaster, William (1983). “The Average Plaquette of $SU(2)$ Gauge Theory on a Body Centered Hypercubic Lattice”. In: *Phys. Rev. D* 28, p. 2076. DOI: 10.1103/PhysRevD.28.2076.